RSC Advances

ROYAL SOCIETY OF CHEMISTRY

www.rsc.org/advances

RSC Advances

RSCPublishing

ARTICLE

Probing 2D sub-bands of bi-layer graphene

Cite this: DOI: 10.1039/xoxxoooooox

Cheng-Wen Huang,[a] Bing-Jie Lin,[a] Sung-Yen Juang,[a] Fu-Yu Shih,[b] Wei-Hua Wang,[b] Chih-Yi Liu[a,c] and Hsiang-Chen Chui[a,c,*]

Received ooth January 2012,
Accepted ooth January 2012

DOI: 10.1039/xoxxoooooox

www.rsc.org/

Investigations of Raman spectra and surface enhanced Raman spectra (SERS) of supported and suspended bilayer graphene were realized. The ability of SERS to greatly enhance the Raman signals is regarded as useful tools, but the dopants induced by the metallic nanoparticles deposition may affect the electron scattering processes. The four 2D sub-bands of bilayer graphene are associated with four-step Stokes-Stokes double-resonance Raman electron scattering processes and can be analyzed by fitting the corresponding Raman peak with muti-Lorentzian functions. To extricate the dopant effect of the substrate from one of metallic nanoparticles, the suspended graphene is adopted here. The enhancements of SERS over Raman spectra are also calculated. For the supported graphene, the SERS enhancement factors of the sub-bands obey 2D22<2D11<2D21<2D12 and exhibit an integrated intensity that is proportional to the Raman cross-section. For suspended graphene, such factors obey 2D11<2D12<2D21<2D22, with 2D12, 2D21, and 2D22 being close to each other because the rate of the scattering for some processes decrease and contribute to another process in the integrated area of Raman signals when the decays happen. The reason responsible for the factor difference is discussed through the presented analysis of the Raman and SERS signals of supported and suspended bilayer graphene.

1. Introduction

Raman and surface-enhanced Raman spectroscopy (SERS) have been extensively used to investigate the vibration properties of materials [1-6]. Recently, they have been utilized as powerful methods for characterizing the interactions of phonons and the band structure of graphene [7-9]. With one to several atomic layers, graphene is the thinnest sp^2 allotrope of carbon, and therefore has many unique and interesting electrical and optical properties [10-12]. The number of layers, defects and dopants, influence the phonon modes of graphene and their effects on its properties can be studied using Raman spectroscopy [13-15]. SERS is an effective tool for investigating the properties of graphene because graphene yields weak Raman signals [7, 8]. Recently, several groups have studied SERS of graphene by the deposition of silver and gold nanoparticles on it [8, 16-19]. The deposition possibly induces the charged dopants. The charged dopants, produced by residual photoresist in the fabrication process, also affect the substrate. Based on relevant studies [20, 21], the properties of metallic particles on graphene that is used as an electrode in an electronic device can be understood clearly and suspended graphene is used to demonstrate the effect of charged dopants of nanoparticle on the graphene.

Interestingly, bilayer graphene has attracted much attention for use in field-effect transistors because of its band gap can be tuned by applying a transverse electronic field [22-27]. In this work, both supported and suspended graphene which were identified as bilayer graphene by Raman spectroscopy and optical microscopy were fabricated by micromechanical cleavage method. After silver nanoparticles were deposited on the samples by thermal deposition, Raman and SERS signals were all obtained by micro-Raman microscopy. The frequencies, intensities, and bandwidths of the four sub-bands, deconvolved with muti-Lorentzian functions from the Raman 2D bands of supported and suspended bilayer graphene, were systematically analyzed. Based on the above results, the enhancement factors of SERS and Raman were calculated and used to demonstrate the mechanism of enhancement by the deposition of metallic nanoparticles on graphene flakes. Under our analysis, details about the effect of charged impurities on the substrate or the dopant effect from silver nanoparticles deposition can be explained. And the change in the integrated areas can be obtained by Raman and SERS measurements. The investigations of Raman and SERS signals of supported and suspended bilayer graphene were realized.

2. Samples preparation and characterization

Suspended graphene was fabricated by mechanical exfoliation of graphene flakes onto an oxidized silicon wafer. First, ordered squares with areas of 6 μm^2 were defined by photolithography on an oxidized silicon wafer with an oxide thickness of 300 nm. Reactive ion etching was then used to etch the squares to a

depth of 150 nm. Micromechanical cleavage of highly ordered pyrolytic graphite was carried out using scotch tape to enable the suspended graphene flakes to be deposited over the indents. To study the SERS, silver nanoparticles were deposited on the graphene flake at a deposition rate of 0.5 nm/min using a thermal deposition system. A 5 nm-thick layer of silver nanoparticles on the graphene flake was thus formed. Since the size, shape, and distribution of metallic particles can influence the enhancement of SERS signals, and therefore the distributions of sizes of silver nanoparticles on supported and suspended graphene can be imaged by scanning electron microscopy, as presented in our previous work[28]. Based on the above results, the particle sizes, shapes, and distributions of the two-types of graphene are similar. An optical micrograph, presented in Figure. 1(a), was used to characterize the suspended graphene. The image shows a clear color difference between monolayer and bilayer graphene.

A micro-Raman microscope (Jobin Yvon iHR550) was utilized to obtain the Raman and SERS signals of bilayer graphene. A 632 nm He-Ne laser served as the excitation light source. The polarization and power of the incident light were adjusted by a half-wave plate and a polarizer. The laser power was monitored using a power meter and kept constant as the measurements were made. The excited laser power was 0.45 mW and 0.06 mW, the integration time was 180s and 60s for Raman and SERS measurement, respectively. Finally, the Raman scattering radiation was sent to a 55-cm spectrometer and a liquid-nitrogen-cooled charge-coupled device (CCD) for spectral recording. Figures. 1(b) and 1(c) present the Raman and SERS signals of supported and suspended graphene under the preset experimental conditions. Figure. 2 shows the frequencies and the full width at half maximum (FWHM), bandwidth, of the G band of the supported and suspended graphene which obtained from Raman and SERS measurements. The peak positions of the G bands of the supported and suspended bilayer graphene were 1576 and 1567 cm^{-1} in the Raman spectra, while those in the SERS were 1579 and 1573 cm^{-1}. The bandwidths of the G bands of supported and suspended graphene were 13 and 21 cm^{-1} for the Raman spectra and 16 and 22 cm^{-1} for the SERS signals. According to previous studies [20, 21], the upshift of the G band reflects doping with charged impurities. The peak position of the G band of the suspended graphene is redshifted comparing to that of supported graphene, consistent with the above expectations. The bandwidth of the G band of suspended graphene was approximately twice that of supported graphene, and this result is similar to one obtained previously [14]. The G band of the supported graphene, obtained from the SERS signals, is blueshifted from that obtained from the Raman signals, and this result is similar to one obtained previously[16]. According to that study, graphene can be doped by depositing silver nanoparticles on its surface [16]. The I_{2D}/I_G ratios and peak positions of G and 2D bands are related to the doping, and the I_{2D}/I_G ratio is more sensitive to the doping than is the peak shift. A lower I_{2D}/I_G ratio is associated with charged impurities in graphene. The I_{2D}/I_G ratios from the Raman over SERS signals of supported graphene are 0.93 and 1.1, while those of suspended graphene are 1.28 and 1.33. Based on the results, the doping effect of supported graphene is stronger than that of suspended graphene.

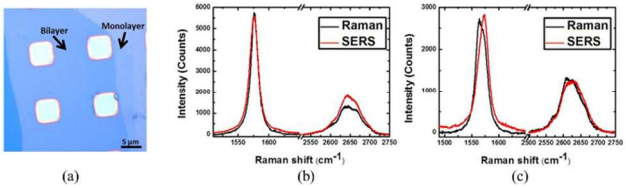

Figure. 1. (a) Optical image of bilayer graphene include suspended and supported graphene, (b) signals of Raman and SERS which are supported graphene, and (c) signals of Raman and SERS which are suspended graphene.

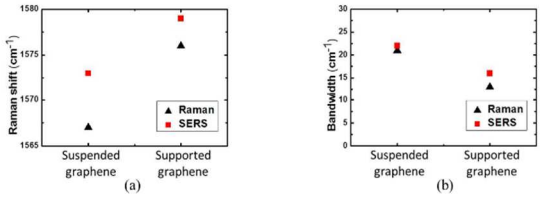

Figure. 2. (a) Peak positions and (b) bandwidths of Raman and SERS signals of supported and suspended graphene identified as bilayer graphene.

3. Results and data analysis

The 2D peak is produced by four-step Stokes-Stokes double-resonance Raman (DRR) scattering[29]. The four sub-bands originate from the dispersion of various phonons. The DRR process provides four ways to connect two points outside or inside electronic dispersion, both of which have been reported upon. After electrons have been excited from π_i to π_i^* (i=1, 2), a total of four possible electron scattering processes can occur [30], as presented in Figure. 3. The four processes are indicated as $2D_{11}$, $2D_{12}$, $2D_{21}$, and $2D_{22}$, respectively. According to previous reviews, the 2D band of the bilayer is anti-symmetric unlike that of monolayer graphene. Ferrari *et al.* [31] explained that the DRR scattering of bilayer graphene is a fourth-order process which involves four virtual transitions. It is caused by the variation in the electronic band structure with the number of graphene layers. To elucidate the specific characteristic of the 2D band, every set of experimental data are deconvolved to four Lorentzian profiles using the scientific data analysis program, Origin 9. Here, the lineshape of each sub-band can be regarded as Lorentzian profiles. Figures. 4(a) and 4(b) plot deconvolutions of Raman and SERS signals of supported graphene by applying multi- Lorentzian functions, while Figures. 4(c) and 4(d) show those of suspended graphene.

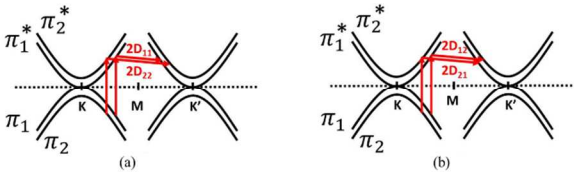

Figure. 3. The four different electron scattering processes of bilayer graphene by DRR scattering. The iTO phonons are involved in the process of $2D_{11}$ and $2D_{22}$ from the (a) symmetric phonon branch, while in the process of $2D_{12}$ and $2D_{21}$ from (b) anti-symmetric phonon branch.

The four sub-bands of supported and suspended graphene, obtained from Raman and SERS measurement of the 2D band ($2D_{11}$, $2D_{12}$, $2D_{21}$, and $2D_{22}$), are deconvolved and shown in Table 1. Here, the uncertainty budget, estimated as 3 cm^{-1}, partially comes from the systematic uncertainty of Raman measurement system, 2 cm^{-1}, and partially due to the data fitting, 1.5 cm^{-1}. Clear differences between the frequencies of these bands of the supported and suspended graphene are obtained by Raman measurement: $2D_{11}$ exhibits the largest shift of approximately 43 cm^{-1}, while $2D_{22}$ exhibits the smallest shift of approximately 8 cm^{-1}. For supported graphene, the differences of the peak positions of 3 sub-bands ($2D_{12}$, $2D_{21}$, and $2D_{22}$) obtained from SERS and Raman are blue-shifted. Another interesting result is the difference between the center frequencies obtained from the Raman and SERS measurements of supported graphene: the shift of $2D_{22}$ is the largest at approximately 22 cm^{-1}, while that of $2D_{11}$ is the smallest at approximately 2 cm^{-1}. We regarded them are at the same peak position because 2 cm^{-1} difference between them exists in the tolerance range of our measurement system. However, no frequency difference exists between the Raman and SERS measurements of four sub-bands of the 2D band for suspended graphene.

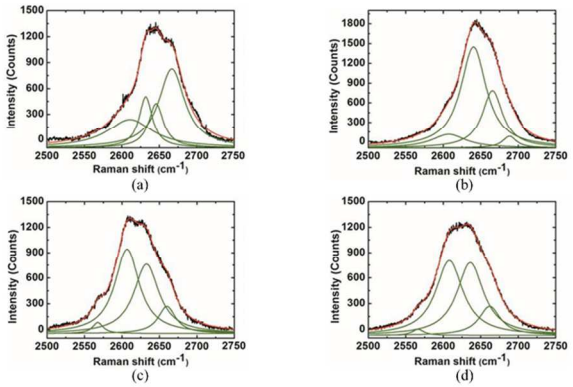

Figure 4. (a) Raman of supported graphene, (b) SERS signals of supported graphene, (c) Raman of suspended graphene, and (d) SERS signals of suspended graphene with muti-Lorentzian functions.

Table 1. Peak positions of Raman and SERS signals of supported and suspended graphene identified as bilayer graphene

Supported	Peak position (Raman) unit: cm^{-1}	Peak position (SERS) unit: cm^{-1}
$2D_{11}$	2611	2609
$2D_{12}$	2632	2640
$2D_{21}$	2646	2666
$2D_{22}$	2668	2690
Suspended	**Peak position (Raman) unit: cm^{-1}**	**Peak position (SERS) unit: cm^{-1}**
$2D_{11}$	2568	2568
$2D_{12}$	2607	2607
$2D_{21}$	2633	2633
$2D_{22}$	2660	2660

To elucidate in detail the sub-band of the 2D band, Figure. 5 shows an analysis using muti-Lorentzian functions of the peak positions, intensities, and bandwidths of supported and suspended graphene based on Raman and SERS measurements. The horizontal axis of all figures represents the sub-bands of 2D, and the red circles and black squares indicate Raman and SERS results, respectively. The intensities of the Raman signals from the sub-bands of supported graphene differ greatly from those of suspended graphene. No obvious difference exists between the Raman and SERS signals of any sub-band by measuring suspended graphene, revealing that the intensities are synchronously enhanced. The enhancements of these intensities will be calculated in greater detail in a later analysis. The bandwidths of the $2D_{12}$ and $2D_{21}$ sub-bands of supported graphene, obtained from the SERS signals, are broader than those obtained from the Raman signals, whereas those of the $2D_{11}$ and $2D_{22}$ sub-bands are smaller. For suspended graphene, the bandwidths of the sub-bands, $2D_{12}$, $2D_{21}$, and $2D_{22}$ that are obtained from SERS signals are slightly larger than those obtained from Raman signals. Based on the above results, a clear different performance between suspended and supported graphene when metallic nanoparticles were deposited on graphene surface reveals the substrate effect is existed. The dopant effect contributed from metallic nanoparticles can be observed when graphene is suspended on the SiO_2/Si substrate, revealing the graphene flake as it covered on the SiO_2/Si substrate directly is strongly influenced by the dopant effect. Actually, two dopant effects from the substrate and metallic nanoparticles on the supported and suspended graphene may change the phonon modes of graphene and can be distinguished in our experimental scheme. And the dopant effect from the substrate on the suspended graphene is very weak compared with supported graphene.

To understand the intensities of the Raman and SERS signals, the factors of supported and suspended graphene are calculated, and presented in Figure. 6. The enhancement factor (E) is defined as $E = \frac{Integrated\ intensity\ (SERS)}{Integrated\ intensity\ (Raman)}$. The factors for $2D_{11}$,

$2D_{12}$, $2D_{21}$, and $2D_{22}$ of supported graphene are 16, 107, 52, and 4.7, respectively, while those of suspended graphene are 14, 24, 26, and 29, respectively. The factors for supported graphene are larger than those for suspended graphene for $2D_{11}$, $2D_{12}$, and $2D_{21}$, while the $2D_{22}$ is smaller.

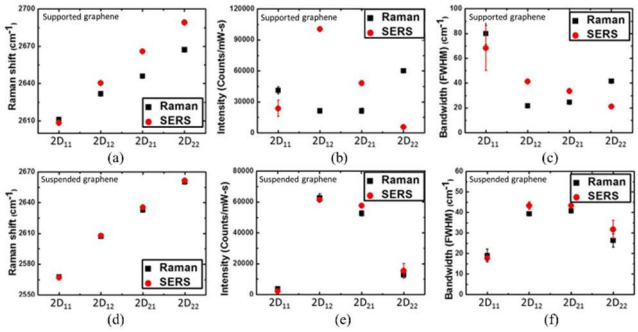

Figure 5. (a)(d) Peak positions of four sub-bands, (b)(e) intensities, (c)(f) bandwidth of supported graphene and suspended graphene include Raman and SERS measurement.

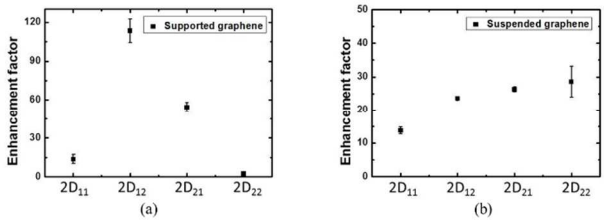

Figure 6. Enhancement factors of (a) supported graphene and (b) suspended graphene.

According to the reviews [30, 32], the integrated area of Raman signals is proportional to its Raman cross section which can be expressed as $\sigma_{ij} \propto H_{ij} \times Q_{ij}$ (i, j = 1, 2). The matrix element H_{ij} is the electron-photon coupling, while the matrix element Q_{ij} is the electron-phonon coupling. Based on the calculations, the integrated area of Raman signals obeys $2D_{22} < 2D_{11} < 2D_{21} < 2D_{12}$. The calculation is highly consistent with the enhancement factor of supported graphene shown by our data.

For suspended graphene, the enhancement factor obtained from the results herein follows the order $2D_{11} < 2D_{12} < 2D_{21} < 2D_{22}$, and $2D_{12}$, $2D_{21}$, and $2D_{22}$ are close to each other. These results are similar to those obtained in a previous study[32], in which Raman signals were obtained with increasing laser power at an excited wavelength of 488 nm. According to Fermi golden rule, the transition rate is proportional to the density of states (DOS). Under our experimental setup, the DOS of π_1^* is larger than the DOS of π_2^* with excited wavelength 633 nm laser[32]. Based on the results, a high decay rate from π_1^* to π_2^* can be expected. During the four-step Stokes-Stokes DRR scattering of 2D peak, the electron is excited by the photon supported by excited laser and it is scattered by the first iTO phonon, and then it can first relax from π_1^* to π_2^*. The electron can relax by emitting a phonon at K' point in a similar process after the first iTO phonon is scattered. Therefore, the rates of the scattering for some processes decrease and contribute to another process in the integrated area of Raman signals when the decays happen. For example, the electron can decay from π_1^* to π_2^* state at the K point before the iTO phonon is scattered. The decay contributes to the increase of the P_{21} and P_{22} processes, while the integrated area of P_{11} peak decreases. When the electron decays from π_1^* to π_2^* at K' point after the iTO phonon is scattered, the processes P_{12} and P_{21} increase, while the integrated area of P_{11} peak decreases. The decay phenomenon also occurs in the other processes such as P_{12}, P_{21}, and P_{22} shown in Figures 7(b)-7(d). The solid lines show the original scattering of the iTO phonon process and the dashed lines show the new possible scattering processes for the electron that can occur after the decay. These results demonstrate why $2D_{22}$ becomes closer to $2D_{12}$ and $2D_{21}$ under the decay mechanism. The substrate effect is responsible for the difference between the performances of supported and suspended graphene.

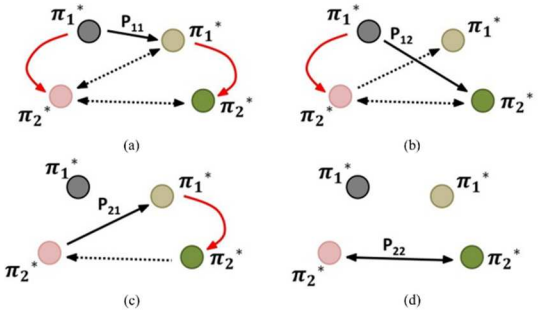

Figure 7. The possible electron decay (red arrows) for processes (a) P_{11}, (b) P_{12}, (c) P_{21}, and (d) P_{22}.

4. Conclusions

Spectroscopic investigation on graphene of the interaction between phonons and electrons with the dopant or the substrate reveals a rich source of interesting physics. Raman and SERS signals of supported and suspended bilayer graphene were obtained. The frequencies, intensities, and bandwidths of four sub-bands were analyzed by systematically deconvolving with muti-Lorentzian functions from 2D bands of supported and suspended graphene. The dopant effect contributed by metallic nanoparticles can be observed when graphene is suspended on the SiO_2/Si substrate, revealing the nanoparticles can strongly doped the graphene surface when the graphene is directly deposited on the SiO_2/Si substrate. Previous studies have calculated and demonstrated the enhancement factors of these sub-bands. The measurements and analysis of the Raman and SERS signals of supported and suspended graphene herein yield a clear understanding of the mechanism of enhancement of bilayer graphene. Therefore, this study provides details of the effect of the substrate effect on charged impurities and the integrated area obtained from Raman and SERS measurements.

Acknowledgements

We wish to acknowledge the support of this work by the Southern Taiwan Science Park Administration (STSPA), Taiwan under contract no. 102CE03 and Ministry of Science and Technology, Taiwan under contact no. NSC 102-2622-E-006-030-CC3. Ted Knoy is appreciated for his editorial assistance.

Notes and references

[a] Department of Photonics, National Cheng Kung University, Tainan 70101, Taiwan.

[b] Institute of Atomic and Molecular Sciences, Academia Sinica, Taipei 10617, Taiwan.

[c] Advanced Optoelectronic Technology Center, National Cheng Kung University, Tainan 70101, Taiwan.

*E-mail:hcchui@mail.ncku.edu.tw

1. W. Suëtaka and J. T. Yates, *Surface infrared and Raman spectroscopy : methods and applications*, Plenum Press, New York, 1995.
2. J. K. Wang, C. S. Tsai, C. E. Lin and J. C. Lin, *J Chem Phys*, 2000, 113, 5041-5052.
3. K. Kneipp, M. Moskovits and H. Kneipp, *Surface-enhanced raman scattering : physics and applications*, Springer, Berlin ; New York, 2006.
4. H. H. Wang, C. Y. Liu, S. B. Wu, N. W. Liu, C. Y. Peng, T. H. Chan, C. F. Hsu, J. K. Wang and Y. L. Wang, *Adv Mater*, 2006, 18, 491-+.
5. C. Y. Liu, M. M. Dvoynenko, M. Y. Lai, T. H. Chan, Y. R. Lee, J. K. Wang and Y. L. Wang, *Appl Phys Lett*, 2010, 96.
6. C. H. Huang, H. Y. Lin, S. T. Chen, C. Y. Liu, H. C. Chui and Y. H. Tzeng, *Opt Express*, 2011, 19, 11441-11450.
7. L. B. Gao, W. C. Ren, B. L. Liu, R. Saito, Z. S. Wu, S. S. Li, C. B. Jiang, F. Li and H. M. Cheng, *Acs Nano*, 2009, 3, 933-939.
8. F. Schedin, E. Lidorikis, A. Lombardo, V. G. Kravets, A. K. Geim, A. N. Grigorenko, K. S. Novoselov and A. C. Ferrari, *Acs Nano*, 2010, 4, 5617-5626.
9. D. Q. Wu, F. Zhang, P. Liu and X. L. Feng, *Chem-Eur J*, 2011, 17, 10804-10812.
10. K. S. Novoselov, A. K. Geim, S. V. Morozov, D. Jiang, Y. Zhang, S. V. Dubonos, I. V. Grigorieva and A. A. Firsov, *Science*, 2004, 306, 666-669.
11. A. K. Geim and K. S. Novoselov, *Nat Mater*, 2007, 6, 183-191.
12. A. K. Geim, *Science*, 2009, 324, 1530-1534.
13. G. Compagnini, G. Forte, F. Giannazzo, V. Raineri, A. La Magna and I. Deretzis, *J Mol Struct*, 2011, 993, 506-509.
14. S. Sahoo, R. Palai and R. S. Katiyar, *J Appl Phys*, 2011, 110.
15. L. G. Cancado, A. Jorio, E. H. M. Ferreira, F. Stavale, C. A. Achete, R. B. Capaz, M. V. O. Moutinho, A. Lombardo, T. S. Kulmala and A. C. Ferrari, *Nano Lett*, 2011, 11, 3190-3196.
16. J. Lee, K. S. Novoselov and H. S. Shin, *Acs Nano*, 2011, 5, 608-612.
17. J. Lee, S. Shim, B. Kim and H. S. Shin, *Chem-Eur J*, 2011, 17, 2381-2387.
18. L. L. Li, B. S. An, A. Lahiri, P. J. Wang and Y. Fang, *Carbon*, 2013, 65, 359-364.
19. A. N. Sidorov, G. W. Slawinski, A. H. Jayatissa, F. P. Zamborini and G. U. Sumanasekera, *Carbon*, 2012, 50, 699-705.
20. C. Casiraghi, S. Pisana, K. S. Novoselov, A. K. Geim and A. C. Ferrari, *Appl Phys Lett*, 2007, 91.
21. Z. H. Ni, T. Yu, Z. Q. Luo, Y. Y. Wang, L. Liu, C. P. Wong, J. M. Miao, W. Huang and Z. X. Shen, *Acs Nano*, 2009, 3, 569-574.
22. A. H. Castro Neto, F. Guinea, N. M. R. Peres, K. S. Novoselov and A. K. Geim, *Rev Mod Phys*, 2009, 81, 109-162.
23. E. V. Castro, K. S. Novoselov, S. V. Morozov, N. M. R. Peres, J. M. B. L. Dos Santos, J. Nilsson, F. Guinea, A. K. Geim and A. H. C. Neto, *Phys Rev Lett*, 2007, 99.
24. F. Bonaccorso, Z. Sun, T. Hasan and A. C. Ferrari, *Nat Photonics*, 2010, 4, 611-622.
25. J. B. Oostinga, H. B. Heersche, X. L. Liu, A. F. Morpurgo and L. M. K. Vandersypen, *Nat Mater*, 2008, 7, 151-157.
26. Y. B. Zhang, T. T. Tang, C. Girit, Z. Hao, M. C. Martin, A. Zettl, M. F. Crommie, Y. R. Shen and F. Wang, *Nature*, 2009, 459, 820-823.
27. T. Ohta, A. Bostwick, T. Seyller, K. Horn and E. Rotenberg, *Science*, 2006, 313, 951-954.
28. C. W. Huang, H. Y. Lin, C. H. Huang, R. J. Shiue, W. H. Wang, C. Y. Liu and H. C. Chui, *Nanoscale Res Lett*, 2012, 7.
29. D. Yoon, H. Moon, Y. W. Son, G. Samsonidze, B. H. Park, J. B. Kim, Y. Lee and H. Cheong, *Nano Lett*, 2008, 8, 4270-4274.
30. J. Jiang, R. Saito, A. Gruneis, G. Dresselhaus and M. S. Dresselhaus, *Chem Phys Lett*, 2004, 392, 383-389.
31. A. C. Ferrari, J. C. Meyer, V. Scardaci, C. Casiraghi, M. Lazzeri, F. Mauri, S. Piscanec, D. Jiang, K. S. Novoselov, S. Roth and A. K. Geim, *Phys Rev Lett*, 2006, 97.
32. D. L. Mafra, J. Kong, K. Sato, R. Saito, M. S. Dresselhaus and P. T. Araujo, *Nano Lett*, 2012, 12, 2883-2887.